High-growth-rate AlGaN buffer layers and atmospheric-pressure growth of low-carbon GaN for AlGaN/GaN HEMT on the 6-in.-diameter Si substrate metal-organic vapor phase epitaxy system

Akinori Ubukata [a],*, Yoshiki Yano [a], Hayato Shimamura [b], Akira Yamaguchi [a], Toshiya Tabuchi [a], Koh Matsumoto [b]

[a] Taiyo Nippon Sanso Corporation, 10 Ohkubo, Tsukuba 300-2611, Japan
[b] TN EMC Ltd., 2008-2 Wada, Tama-city, Tokyo 206-0001, Japan

ARTICLE INFO

ABSTRACT

In this study, we investigated the effects of growth pressure on incorporation of carbon in GaN and on the growth rate of AlGaN using a multiwafer (7×6 in.) mass-production metal-organic vapor phase epitaxy (MOVPE) reactor. In the two-dimensional electron gas (2DEG) region of an AlGaN/GaN high electron-mobility transistor (HEMT) structure, a high GaN purity is required. The incorporation of carbon in GaN could be easily controlled over a carbon concentration range of three orders of magnitude by varying pressure. Thus, the reactor can be used for growth at both reduced pressure and atmospheric pressure. Furthermore, an AlGaN growth rate of over $1 \mu m/h$ was demonstrated for Al composition in the range of 0.3–0.8 by suppressing the gas-phase prereaction between the precursor materials. An AlGaN/GaN HEMT structure was also demonstrated. The magnitude of wafer bowing was less than 50 µm. The full widths at half maximum (FWHMs) of the X-ray rocking curve (XRC) of GaN were 570″ in the GaN (002) direction and 760″ in the GaN (102) direction. The sheet carrier density and Hall mobility were $1.056 \times 10^{13} cm^{-2}$ and 1550 cm^2/V s, respectively.

1. Introduction

There has been considerable interest in the growth of GaN on Si as the most important semiconductor next to silicon because of its applications in solid-state lighting and high-power switching devices [1–3]. Excellent GaN power devices that break the silicon limit have been demonstrated by other groups [4–8]. To reduce the manufacturing cost of GaN power devices, the GaN-on-Si approach has attracted the industry's attention because silicon substrates are inexpensive, and available in large sizes, and can also be readily applied to conventional production lines for GaAs or Si devices. Recently, GaN layers grown on 6- and 8-in.-diameter silicon substrates have been reported [9–13].

There is still a problem in the growth of AlGaN or AlN since a gas-phase prereaction occurs between precursors and NH$_3$ rather than with other precursor materials [14]. This prereaction between trimethylaluminum (TMA) and NH$_3$ readily occurs at high TMA and NH$_3$ flow rates or at a high growth pressure, which leads to a considerable reduction in the growth rate and Al composition in solid AlGaN. The growth of Al-related materials at a low rate and reduced pressure has less risk, so the effect of a gas-phase prereaction can be avoided. On the other hand, a high

throughput is a considerable issue in GaN power switching devices. One of our objectives is to enable the atmospheric-pressure growth and achieve a higher growth rate of AlGaN or AlN using a large reactor by overcoming the gas-phase prereaction issue. Note that growth pressure is a useful growth parameter for controlling the defect density and impurity level in GaN. The use of a large high-throughput reactor has contributed to the reduction in wafer cost; however, the issue of the high growth rate still remains because of the effect of the gas-phase prereaction [15].

In this study, the growth of a crack-free HEMT structure on 6-in. silicon substrates was demonstrated using a multiwafer reactor. In such a structure, a GaN layer was grown near atmospheric pressure at a higher rate than in a previous report [16]. To reduce wafer cost, growth rate was maintained not to decrease in controlling carbon concentration of the GaN buffer. It is not so easy to grow GaN at near-atmospheric pressure using such a tool because of the influence of the gas-phase prereaction. As substrate size is scaled up, the requirement for good wafer flatness becomes stricter owing to the limited tolerance to wafer bowing in the processing of a full wafer.

2. Experiments

In this study, experiments on growth were conducted using an MOVPE reactor used for production with a capacity of 7×6 in.

(Taiyo Nippon Sanso Co., UR25K), which was developed for the manufacture of LEDs and electron devices. The precursors are supplied from the bottom of the reactor and then injected into the reaction zone from a trilayer nozzle at the center of the reactor. Wafers are rotated in a planetary motion. The wafer holder disc is heated by resistance heaters, which are controlled separately in each zone. The top ceiling disc made of quartz and the wafer holder disc are automatically transferred and replaced by a robot arm. The typical growth pressures were 13 kPa for AlN and SL, and 90 kPa for GaN. The V/III ratios were 190 for AlN and 3000 for AlGaN and GaN. Six-inch-diameter (111) Si wafers with a thickness of 675 μm were used as substrates. In the MOVPE reactor, the injection nozzle is designed for a high flow speed which enables the suppression of undesirable parasitic reactions in the vapor phase without causing turbulence. The design criteria of the reactor for suppressing parasitic reactions were described in a previous paper [17]. Trimethylgallium (TMG), TMA and ammonia (NH_3) were used as source gases of Ga, Al and N, respectively. To observe wafer bowing during growth, a curvature monitor (Laytec Epicurve®TT) employing laser reflection was installed on the top lid of the reactor. Detailed operating principles of the monitor can be found in the literature [13]. High-resolution X-ray diffractometry (HRXRD) was then conducted using a Bruker-AXS Vantec D8 diffractometer. Hall mobility and Hall carrier concentration were measured using a Nanometrics Hall measurement system. Carbon and oxygen concentrations were measured by SIMS.

3. Results and discussion

In this experiment, a high-flow-velocity reactor was used to suppress gas-phase prereactions. Since the gas-phase prereaction between NH_3 and TMA is the most considerable among those between the other source materials, the growth of AlN and AlGaN single layers was initially investigated to examine whether a gas-phase parasitic prereaction was significant. Fig. 1 shows the rate of AlN growth at 1080 °C at a V/III ratio of 190 and a growth pressure of 13 kPa. The growth rate of AlN linearly increased with the amount of TMA input. The growth rate did not saturate even when it reached 1.4 μm/h. Fig. 2 shows the Al content of solid AlGaN as a function of TMA partial pressure [TMA/(TMA+TMG)] at a growth rate of over 1 μm/h. Because of the suppression of the prereaction in the reactor, we obtained a growth rate of 1.86 μm/h for $Al_{0.6}Ga_{0.4}N$. To our knowledge, this is the highest growth rate of AlGaN using a multiwafer 6 in. reactor.
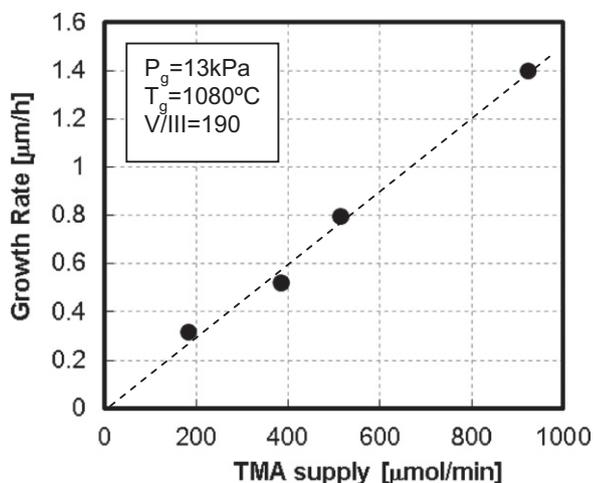

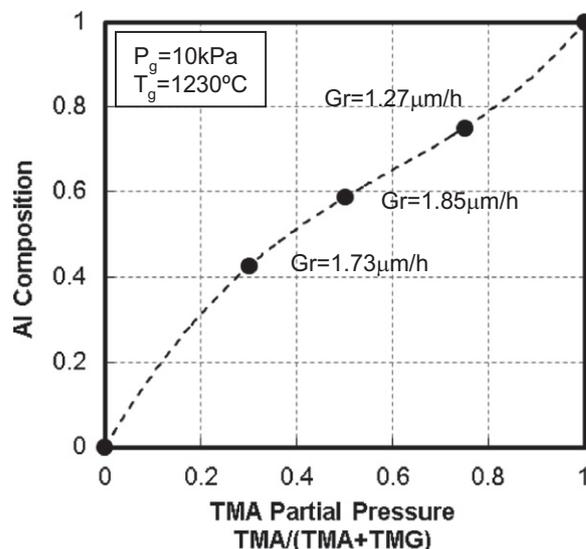Fig. 1. Growth rate of AlN grown at 1080 °C with a V/III ratio of 190.

Fig. 2. Al composition in solid AlGaN as a function of TMA/(TMA+TMG).

According to the report by Nakamura et al., some adducts assume the transition state with a bimolecular reaction [18]. In this transition state, a molecule with one N atom and two adducts forms. One H atom coupled with one N atom is combined with methyl alkyls by organometals. 4-H molecules combine with 1-C, and the molecule formed separates from the adducts. These bimolecules or trimolecules combine in sequence with adducts by the same transition procedure. In the TMA case, the potential energy of the transition state is relatively lower than that of the initial state so that adducts are excited to their transition states. This transition procedure does not revert easily, that is it is irreversible. On the other hand, the potential energy for TMG is relatively lower than that in the initial stage so that the adducts formed will decompose easily. Thus, it is possible for the adducts to revert to their initial forms, which are unique and isolated. In the TMG case, it is less likely to go into the transition state and to finally undergo bimolecular or trimolecular reactions.

The crystal quality of AlGaN was determined by the time the adduct takes to go through the wafer. There are many reports on high quality AlN grown using a small reactor operated at a high flow velocity as one of the growth conditions [19–21]. In the case of using a large reactor, only flow velocity maintenance is insufficient to obtain good-crystal-quality AlN in the entire wafer because the material density in the upstream region is very high. In this case, ammonia and metal organic materials such as TMA were separately introduced into the reactor without turbulence to prevent the easy occurrence of gas-phase prereactions. The FWHM of the XRC for the AlN (0002) direction is typically 900″ at a thickness of 300 nm.

Fig. 3 shows the dependence of the carbon concentration of GaN on V/III ratio. The carbon concentration decreased by one order of magnitude when V/III ratio was increased tenfold. When growth pressure was increased from 13 kPa to atmospheric pressure, the carbon concentration was decreased by two orders of magnitude or more. The concentration of carbon impurities that originate from decomposed precursors depends on growth pressure. However, upon decreasing the carbon concentration by increasing V/III ratio, the growth rate decreased to less than 0.6 μm/h, which was limited by the maximum NH_3 flow rate. Thus, the atmospheric-pressure growth of GaN is one of the solutions to obtaining low-carbon-concentration GaN. The carbon concentration of AlGaN as a function of V/III ratio is also plotted in Fig. 3. The Al composition in AlGaN samples was in the range of
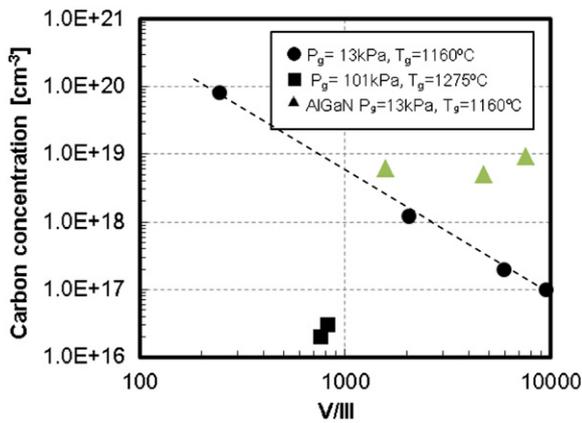
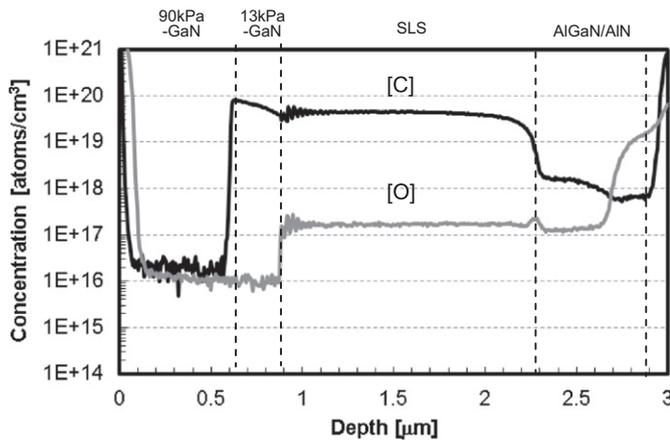Fig. 3. Carbon concentrations in GaN and AlGaN as a function of V/III ratio.

Fig. 4. SIMS depth profiles of carbon and oxygen in HEMT structure.

0.2–0.25 and the growth rate was 0.3 μm/h. No effect of V/III ratio on the carbon concentration was observed in this V/III range.

A HEMT structure was grown on a Si (111) substrate. Nucleation layers consisted of a 150-nm-thick AlN layer, followed by a 250-nm-thick AlGaN layer for controlling wafer bowing and an (AlN/AlGaN) SL grown at a pressure of 13 kPa for suppressing crack formation. Then, a 350-nm-thick ud-GaN layer was grown at 13 kPa, followed by a 700-nm-thick layer of ud-GaN at 90 kPa to reduce the carbon concentration close to that in the two-dimensional electron gas (2DEG) region. Then, a 20-nm-thick $Al_{0.25}Ga_{0.75}N$ layer as the barrier layer and an ud-GaN cap layer were grown. Crack-free HEMT structures with thickness of up to 6 μm were obtained by optimizing the SL structure buffer technique [22]. The FWHMs of the XRC of the GaN layers were 570″ in the GaN (002) direction and 760″ in the GaN (102) direction. The sheet carrier density, Hall mobility and sheet resistance obtained by Hall measurement were 1.056×10^{13} cm^{-2}, 1550 cm^2/V s and 382.4 Ω/□, respectively.

It is well known that there is a means of growing semi-insulating GaN buffer layers by controlling the size of nucleation sites in the case of GaN on sapphire substrates [23]. In this case, GaN nucleation size was controlled by the two-step growth temperature technique. Note that semi-insulating GaN films are obtained with the formation of electron traps at defects. They are also usually doped to compensate for any free carriers [24]. One possible dopant is carbon, whose diffusion coefficient is relatively low in GaN. According to Kato et al., the breakdown voltage of electronic devices increased with the carbon concentration of GaN [25]. Fig. 4 shows the SIMS depth profile of the HEMT structure. The carbon concentration of a highly resistive GaN layer was in the range of 10^{19} cm^{-3}. Again note that impurities in

a GaN buffer grown at 90 kPa, which is next to an AlGaN barrier layer, have to be eliminated to avoid impurity scattering [26]. Since it is important to reduce wafer cost, we did not decrease the growth rate of the GaN layers by changing growth pressure by controlling the carbon concentration. By photoluminescence measurement, the emission intensity of the yellow band originating from carbon-related deep levels was found to be less than 1% of that of GaN band edge. It is supposed that nitrogen vacancies are almost compensated for by carbon. In Fig. 4, a good stiffness of carbon concentration is shown at the interface where growth pressure was changed in the GaN buffer. The slope of the carbon concentration at the interface of GaN corresponds to that of the growth time of GaN during the growth pressure change. The carbon concentration of the GaN layer grown at 13 kPa increased with an increase in growth thickness. This is due to the reduced surface substrate temperature caused by wafer bowing because the wafer becomes convex with compressive strain during GaN growth. Carbon incorporation efficiency is strongly dependent on temperature since it is related to TMG decomposition mechanism. The average growth rates of the SL and GaN were 2 μm/h and 3 μm/h, respectively. Average growth rate increased linearly with TMG input up to 10 μm/h without saturation even with atmospheric-pressure growth. This is cost-effective in terms of wafer manufacture as it entails no decrease in growth rate by controlling only carbon concentration. Oxygen concentration was almost the same in AlGaN or AlN layers. It is assumed that oxygen comes from TMA. When the growth temperature of GaN was increased to more than 20 °C, residual oxygen level was decreased by half.

An example of the wafer curvature during the growth of a HEMT with a total thickness of 2.8 μm is shown in Fig. 5. The vertical axis shows the difference between the top and bottom heights of the wafer. The silicon wafer was concave owing to the tensile strain in AlN. The growth stress was negligible in the AlGaN nucleation step owing to compressive strain. During the SL growth steps, compressive stress was further introduced. The inset shows the wafer curvature data for different SL growth temperatures. The growth stress further decreased with an increase in temperature at the end of the SL steps. The lower the SL growth temperature, the flatter the wafer became at the end of the SL step. It is supposed that the nucleation site in the case of AlN in the SL is smaller at 1090 °C and further induces partial relaxation. In this experiment, a flat wafer was obtained at room temperature when the SL was grown at 1170 °C. The GaN growth was divided into two steps. In the first step, a 300 nm-thick GaN layer was grown at 13 kPa to serve as a semi-insulator; in the second step, a 600 nm-thick GaN layer was grown at 90 kPa for reducing carbon. During postgrowth cooling, the growth stress became positive owing to the difference in thermal expansion. The final magnitude of wafer bowing at room temperature was approximately 30 μm with a concave shape. A
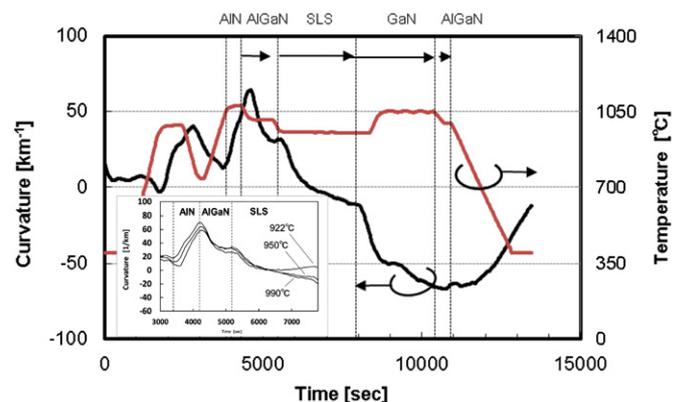

Fig. 5. Wafer curvature during HEMT growth.

detailed discussion of the mechanism of bowing control will be given in our future paper. If the magnitude of wafer bowing increases during growth, the temperature difference between the edge and center of the wafer becomes larger and the thickness or Al composition distribution in a wafer will be affected. Thus, it is important to control wafer stress and the temperature distribution of the wafer holder on which 6-in. Si substrates are placed. To minimize the temperature variation of the 6-in. wafers, the heater was divided into six zones, which were controlled separately in a stepwise manner during the growth. This will be useful for controlling the temperature distribution regardless of growth temperature.

4. Conclusion

The growth of an AlGaN/GaN HEMT structure on a 6-in.-diameter Si substrate was demonstrated using a multiwafer MOVPE reactor used for the mass production. The incorporation of carbon in GaN could be easily controlled over a carbon concentration range of three orders of magnitude by varying pressure. Thus, the reactor can be used for growth at both reduced pressure and atmospheric pressure. Furthermore, an AlGaN growth rate of over 1 μm/h was demonstrated for Al composition in the range of 0.3–0.8 by suppressing the gas-phase prereaction between the precursor materials.

Acknowledgment

References

[1] C. Jun, Z. Shuming, Z. Baoshun, Z. Jianjun, F. Gan, D. Lihong, W. Yutian, Y. Hui, Z. Wenchen, Science in China Series E 46 (2003) 620.
[2] A.E. Wickenden, D.D. Koleske, R.L. Henry, R.J. Gorman, M.E. Twigg, M. Fatemi, J.A. Freitas Jr., W.J. Moore, Journal of Electronic Materials 29 (2000) 21.
[3] A.E. Wickenden, D.D. Koleske, R.L. Henry, M.E. Twigg, M. Fatemi, Journal of Crystal Growth 260 (2004) 54.
[4] Y. Uemoto, T. Morita, A. Ikoshi, H. Ueda, H. Matsuo, J. Shimizu, M. Hikita, M. Yanagihara, T. Ueda, T. Tanaka, D. Ueda, IEDM Technical Digest (2009) 1.
[5] Y. Wu, M. Jacob-Mitos, M.L. Moore, S. Heikman, IEEE Electron Device Letters 29 (2008) 824.
[6] N. Ikeda, Y. Niiyama, H. Kambayashi, Y. Satoh, T. Nomura, S. Kato, S. Yoshida, Proceedings of the IEEE 98 (2010) 1151.
[7] S. Iwakami, O. Machida, M. Yanagihara, T. Ehara, N. Kaneko, H. Goto, A. Iwabuchi, Japanese Journal of Applied Physics 46 (2007) L587.
[8] Y. Dora, A. Chakraborty, L. McCarthy, S. Keller, S.P. DenBaars, U.K. Mishra, IEEE Electron Device Letters 27 (2006) 713.
[9] A. Ubukata, K. Ikenaga, N. Akutsu, K. Matsumoto, T. Yamazaki, T. Egawa, Journal of Crystal Growth 298 (2007) 198.
[10] A.R. Boyd, S. Degroote, M. Leys, F. Schulte, O. Rockenfeller, M. Luenenbuerger, M. Germain, J. Kaeppeler, M. Heuken, Physica Status Solidi C 6 (2009) s1045.
[11] A. Dadgar, et al., Journal of Crystal Growth 297 (2006) 279.
[12] J. Li, et al., Applied Physics Letters 88 (2006) 171909.
[13] D. Zhu, C. McAleesea, Proceedings of the SPIE 7231 (2009) 723118.
[14] K. Matsumoto, A. Tachibana, Journal of Crystal Growth 272 (2004) 360.
[15] J. Selvaraj, S.L. Selvaraj, T. Egawa, Japanese Journal of Applied Physics 48 (2009) 121009.
[16] M. Dauelsberg, D. Brien, R. Pusche, O. Schon, E.V. Yakovlev, A.S. Segal, R.A. Talalaev, Journal of Crystal Growth 315 (2011) 224.
[17] T. Tokunaga, Y. Fukuda, A. Ubukata, K. Ikenaga, Y. Inaishi, T. Orita, S. Hasaka, Y. Kitamura, A. Yamaguchi, S. Koseki, K. Uematsu, N. Tomita, N. Akutsu, K. Matsumoto, Physica Status Solidi (2008) 3017.
[18] K. Nakamura, O. Makino, A. Tachibana, K. Matsumoto, Journal of Crystal Growth 611 (2000) 514.
[19] Y. Ohba, H. Yoshida, R. Sato, Japanese Journal of Applied Physics 36 (1997) L1565.
[20] H. Hirayama, S. Fujikawa, N. Noguchi, J. Norimatsu, T. Takano, K. Tsubaki, N. Kamata, Physica Status Solidi A 206 (6) (2009) 1176.
[21] R. Miyagawa, S. Yang, H. Miyake, K. Hiramatsu, Physica Status Solidi 8 (7–8) (2011) 2069.
[22] T. Suzue, M. Suzuki, Y. Nomura, T. Egawa, The Institute of Electronics, Information and Communication Engineers 108 (323) (2008) 137.
[23] J.H. Lee, M.B. Lee, S.H. Hahm, Y.H. Lee, J.H. Lee, Y.H. Bae, H.K. Cho, MRS Internet Journal of Nitride Semiconductor Research 8 (2003) 5.
[24] H. Tang, J.B. We bb, J.A. Bardwell, R.J. Salzman, C. Uzan-Saguy, Applied Physics Letters 78 (2001) 757.
[25] S. Kato, Y. Satoh, H. Sasaki, I. Masayuki, S. Yoshida, Journal of Crystal Growth 298 (2007) 831.
[26] J. Selvaraj, S.L. Selvaraj, T. Egawa, Japanese Journal of Applied Physics 48 (2009) 121009.